Time-Dependent Density Functional Theory Calculations of Ehrenfest Dynamics of Laser Controlled Dissociation of NO^+: Pulse Length and Sequential Multiple Single-Photon Processes

Wenkel Liang, Christine M. Isborn, Alex Lindsay, and Xiaosong Li*

University of Washington, Department of Chemistry, Box 351700, Seattle, Washington 98195-1700

Stanley M. Smith and Robert J. Levis

Temple University, Department of Chemistry, Philadelphia, Pennsylvania 19122

Received: March 5, 2010; Revised Manuscript Received: April 22, 2010

Intense laser field controlled dissociation reactions of the nitric oxide cation (NO^+) are studied by ab initio Ehrenfest dynamics with time-dependent density functional theory. Intense electric fields with five different pulse lengths are compared, combined with potential energy surface and density of state analysis, to reveal the effect of pulse length on the control mechanism. Controllable dissociative charge states are observed, and the correlation between the laser pulse length and the probability of sequential multiple single-photon processes is presented. This work introduces a concept of using laser pulse length to control the sequential multiple single-photon process.

I. Introduction

Advanced laser techniques, such as ultrashort laser pulses, high-intensity electric fields, pulse shaping, and multiwave mixing, are able to provide increasing control of molecular electronic and vibrational excitation of target states.[1,2] Although these advances offer possibilities to use tailored electromagnetic fields to control the outcome of a chemical reaction via a desired pathway,[3−18] the underpinnings of many laser control mechanisms still remain unclear. The difficulty lies in the complexity of the laser−molecule interaction. For example, just a few of the phenomena necessary to account for mechanism include the time-dependent Stark shift of the potential energy surfaces (PESs), possible multiphoton processes when intense laser fields are used, and nonadiabatic excitation of electronic states. Simple PES modeling is not sufficient, and nonadiabatic electron dynamics are necessary. This complexity thus motivates the use of time-domain approaches to understand some aspects laser−molecule interactions and their effects on the outcome of molecular reactions. It is for this purpose that we developed ab initio Ehrenfest dynamics with TDHF[19] and TDDFT[20] as a computationally inexpensive alternative to full time-dependent Schrodinger equation (TDSE) approach. This approach has been successfully used to study nonadiabatic electronic dynamics and surface collisions.[21−23] More recently, we showed that the Ehrenfest dynamics are able to provide insights into laser−molecule interactions governing reaction channels distribution.[24] In particular, the effect of the polarization of the applied field with respect to the molecular axis on the probability for reaction channels population was demonstrated via access of different PESs.

The goal of the present study is to understand the role of pulse length in the control mechanism. We present a theoretical investigation of the laser-controlled reactions through Ehrenfest/TDDFT calculations of the dissociation of the NO^+ molecule. The study of NO/NO^+ has been an intense area of research for both experiment[25−27] and theoretical calculation[28−30] due to the physical and chemical processes occurring in the upper atmosphere and pollution problems. In this paper, we will focus on using laser radiation to control product charge states with the combined techniques of nonadiabatic dynamics and PES analysis. In particular, we address the laser pulse length control of sequential photon absorption processes and provide insight into possible control schemes to aid in further understanding of the mechanisms of a photoinduced dissociation.

II. Method

As the details of the TDHF/TDDFT Ehrenfest dynamics using a triple-split operator approach have been derived, implemented, and tested in previous publications,[19,20] we only provide a brief review here. In the density matrix formalism of TDHF/TDDFT, the time-dependent equation is,

$$i\frac{\mathrm{d}\mathbf{P}}{\mathrm{d}t} = \mathbf{KP} - \mathbf{PK} \tag{1}$$

where **P** and **K** are the density and Kohn−Sham matrices, respectively, in an orthonormal basis. The electronic degrees of freedom are propagated with a modified midpoint and unitary transformation method (MMUT),[31]

$$\mathbf{C}^{\dagger}(t_k)\cdot\mathbf{K}(t_k)\cdot\mathbf{C}(t_k) = \varepsilon(t_k) \tag{2}$$

$$\mathbf{U}(t_k) = \exp[i\cdot 2\Delta t_e\cdot\mathbf{K}(t_k)] = \mathbf{C}(t_k)\cdot\exp[i\cdot 2\Delta t_e\cdot\varepsilon(t_k)]\cdot\mathbf{C}^{\dagger}(t_k) \tag{3}$$

where Δt_e is the time step for the MMUT integrator. Since the propagator in eq 3 is constructed at t_k, the midpoint between densities at t_{k-1} and t_{k+1}, the actual time step becomes $2\Delta t_e$ to

* To whom correspondence should be addressed. E-mail: li@chem.washington.edu.

10.1021/jp102013b
Published on Web 05/07/2010

propagate the density matrix from time t_{k-1} to t_{k+1} with a fixed nuclear position,

$$\mathbf{P}(t_{k+1}) = \mathbf{U}(t_k)\cdot\mathbf{P}(t_{k-1})\cdot\mathbf{U}^{\dagger}(t_k) \tag{4}$$

Because the electronic wave function changes much faster than the nuclear motion, the nuclear position coupled midpoint Fock/Kohn−Sham propagator updates the integrals required in the Fock/Kohn−Sham matrix with the second kind of time step Δt_{Ne}, which encompasses $m\Delta t_e$ iterations. The integrals are recomputed at the midpoint of every Δt_{Ne} time step, $t' + (\Delta t_{Ne})/2$, and are used in the Fock/Kohn−Sham matrix $\mathbf{K}_0$ for the m MMUT steps between t' and $t' + \Delta t_{Ne}$:

$$\mathbf{K}_0(t) = \mathbf{h}\left[x\left(t' + \frac{\Delta t_{Ne}}{2}\right)\right] + \mathbf{G}_{xe}\left[x\left(t' + \frac{\Delta t_{Ne}}{2}\right), \mathbf{P}(t)\right] \tag{5}$$

where $\mathbf{h}$ and $\mathbf{G}_{xe}$ are one and two electron matrices, respectively. The nuclear position is updated for n Δt_{Ne} time steps before the reevaluation of gradient, which occurs in the third time step $\Delta t_N = n\Delta t_{Ne}$. Velocity Verlet is used to propagate the nuclear coordinates,

$$p(t_{k+1/2}) = p(t_k) - \frac{1}{2}g(t_k)\cdot\Delta t_N \tag{6}$$

$$x(t_{k+1}) = x(t_k) + \frac{p(t_{k+1/2})}{M}\cdot\Delta t_N \tag{7}$$

$$p(t_{k+1}) = p(t_{k+1/2}) - \frac{1}{2}g(t_{k+1})\cdot\Delta t_N \tag{8}$$

where p is the momenta, and g is the energy gradient.

The time-dependent Kohn−Sham Hamiltonian includes the electron-field coupling term within the electric-dipole approximation,

$$\mathbf{K}(t) = \mathbf{K}_0(t) + \mathbf{d}\cdot e(t) \tag{9}$$

where $\mathbf{K}_0$ is the field-free Fock/Kohn−Sham matrix, and $d_{\mu\nu} = \langle\chi_\mu|r|\chi_\nu\rangle$ is the dipole integral in the AO basis. We use a linearly polarized and spatially homogeneous external field of frequency ω and maximum field strength E_{max},

$$e(t) \approx E_{max}\sin(\omega\cdot t) \tag{10}$$

As a result of eq 8, at any given time during the simulation, the total energy of the system including the electron-field coupling can be written as,

$$E(t) = Tr\left[\mathbf{P}(t)\cdot\left(\mathbf{K}(t) - \frac{1}{2}\mathbf{G}(t)\right)\right] = E_{mol}(t) + \mu(t)\cdot e(t) \tag{11}$$

where we define E_{mol} as the field-free energy of the molecule, and μ is the instantaneous dipole.

In the current implementation of the TDDFT Ehrenfest dynamics, atom-centered basis functions are used in the MO expansion. As a result, electronic ionizations cannot be modeled directly. On the other hand, the focus of this work is to illustrate the crucial role of laser pulse length in the photoabsorption processes during the course of dissociative reaction. The discussions as presented in the next section will focus on preionization processes.

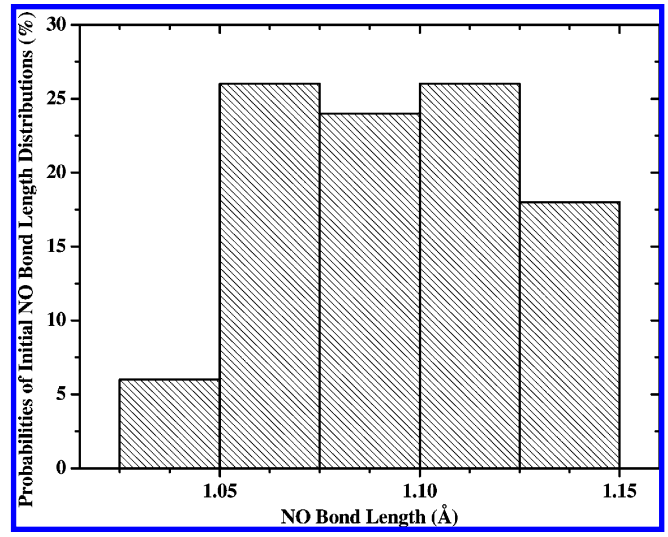

Figure 1. Boltzmann 298 K distribution of initial N−O bond lengths. A total number of 50 initial conditions are sampled. The BLYP/6-31++G(d,p) optimized bond length is 1.08 Å.

III. Results and Discussion

The modified development version of the GAUSSIAN[32] series of programs was used to carry out all computations in the present investigation. The BLYP functional with the 6-31++G(d,p) basis set is used for calculations of ground state properties and excited states within the linear response framework[33,34] and is implemented with the Ehrenfest dynamics approach as described above for laser-controlled electron−molecule dynamics. In the Ehrenfest dynamics, a step size of $t_N = 0.10$ fs is used for the velocity Verlet, with $t_{Ne} = 0.01$ fs for the midpoint Kohn−Sham integrator, and $t_e = 0.001$ fs for the MMUT step. Tests showed that these time steps conserve the energy of the system (after the field is removed) to within 10^{-4} Hartree and represent a reasonable combination of accuracy and computational cost. A linearly polarized and spatially homogeneous light pulse was applied for interaction time periods, ranging from 20 to 100 fs. The light polarization, within the dipole approximation (eq 10), is aligned with the molecular axis. After the laser field is turned off, the simulation continues until $t = 150$ fs. At the end of the simulation, the N−O bond is considered broken if the distance between atoms exceeds 3 Å.

A total of 50 trajectories were integrated for each set of field parameters. Initial conditions were chosen for the NO^+ molecule to simulate a Boltzmann ensemble of harmonic oscillators at room temperature (298 K). For a specific vibrational mode with a given vibrational energy, the initial phase was chosen randomly and classically. The total angular momentum was set to zero. Since the actual potential energy surface is not strictly harmonic, the initial vibrational coordinates and momenta generated by this procedure were scaled to correct for the anharmonicity.[35] A similar approach has been implemented for studies of laser-induced dissociation of acetylene dication.[24] Figure 1 shows the room temperature Boltzmann distribution of the initial N−O bond lengths, which are within about ±0.08 Å of the equilibrium bond length of 1.08 Å.

In an earlier study, we have shown that the probability of laser control of molecular reaction strongly depends on the

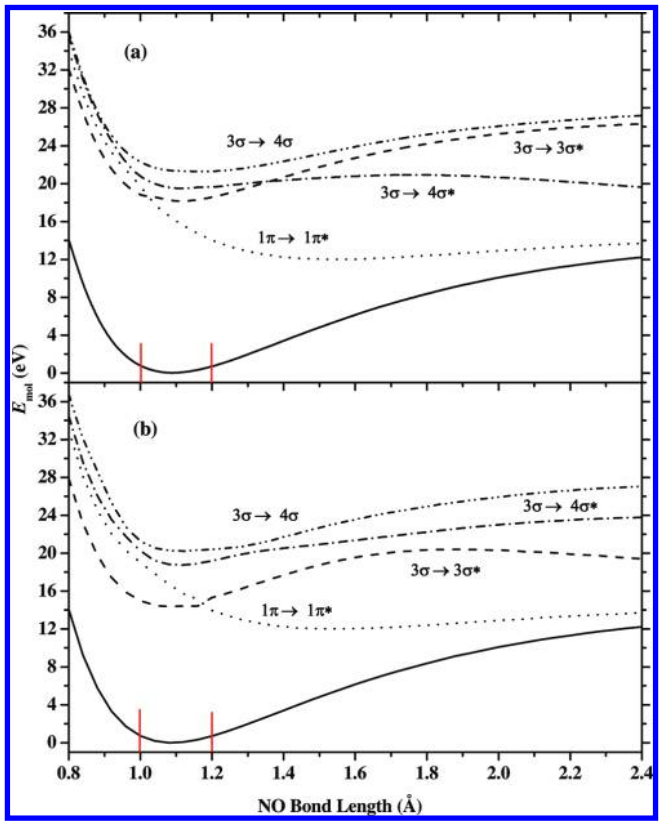

Figure 2. Lowest electric-dipole allowed transitions: (a) field-free PES and (b) field-dressed PES with a static electric field of $E = 0.05$ au applied along the molecular axis. Red lines indicate the range of bond lengths within the room temperature Boltzmann distribution. The $\pi \rightarrow \pi^*$ transition has an oscillator strength of ~0.7.

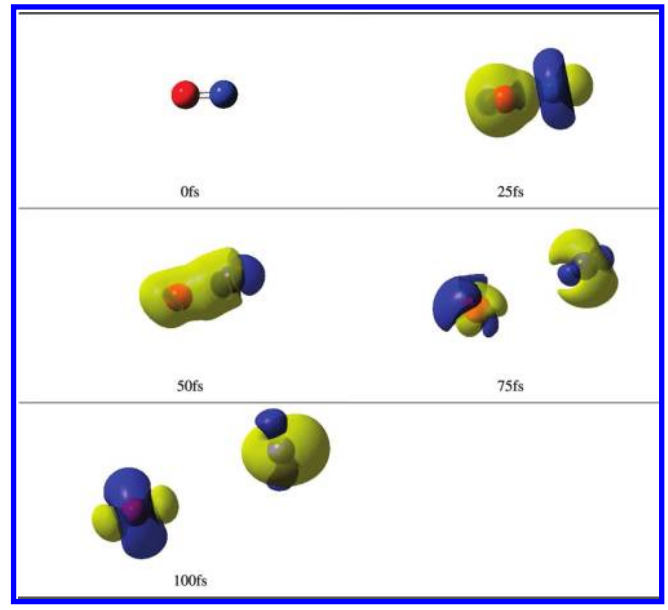

Figure 3. Snapshots of charge density distribution at $t = 0$, 25, 50, 75, and 100 fs. Blue and yellow coded areas represent negative and positive charge distributions, respectively. Relative charge distributions at the end of the trajectories are used to identify dissociative reaction channels.

oscillator strength of the electronic transition. For polarizations perpendicular to the NO^+ molecular axis, the lower lying electronic transitions are only weakly allowed (oscillator strength $f < 0.02$) and the PESs are attractive in nature. Therefore, in this study we only focus on situations where the laser polarization is aligned with the molecular axis. Figures 2a shows several PESs for lowest dipole-allowed electronic transitions along the molecular axis, obtained with linear response TDDFT. Figure 2b shows the same set of PESs computed with a static electric field of $E = 0.05$ au within the perturbative linear response theory. Although the electronic system in such an electronic field is beyond the perturbative regime, the PES obtained still can provide some insights into the control mechanism. The lowest energy excited state corresponds to the $\pi \rightarrow \pi^*$ electronic transition. Although the PES of this excited state is slightly attractive, the oscillator strength of the excitation is very large ($f \sim 0.7$), making it a good candidate as the target *doorway* state, which provides possibilities to access higher lying excited states via sequential photon absorption process. As shown in Figure 2a, within the Boltzmann sampled bond lengths, this doorway state is accessible with a resonant photon frequency of $\omega = 0.60$ au (16.3 eV), and, therefore, we choose this frequency of light in the following simulations. Because Figure 2b indicates that application of a static external field of $E = 0.05$ au significantly changes the characteristics of the PES, real-time electronic−molecular dynamics is needed to provide a better understanding of laser control.

Figure 3 schematically shows snapshots of the time-dependent charge density distribution taken from one representative laser-controlled dissociative reaction. Time-dependent charge density is defined as, $\Delta\rho(t) = \rho(t) - \rho_0(t)$, where $\rho(t)$ and $\rho_0(t)$ are TDDFT and ground state electron densities at time t. Blue and yellow coded surfaces represent electron populating and depopulating regions, respectively, as compared to the ground state configuration. At $t = 0$, the electron wave function starts in the ground state. As the field is turned on, electrons are driven into the excited state while the bonding orbital gradually loses electron populations. At $t = 50$ fs, most of the electrons in the bonding orbital are excited to high-lying molecular orbitals, and the molecule starts to dissociate during the period of 50−75 fs. At $t = 100$ fs, the N and O atoms are already well separated, with the oxygen atom gaining electrons during the dissociative process.

Since the TDDFT Ehrenfest dynamics is a mean-field theory, atomic and molecular properties represent average values even at the asymptotic dissociation limit. Nevertheless, a qualitative understanding of the laser-controlled dissociative charge state can be obtained from analyzing the charge distribution at the end of the dynamics. For example, if the nitrogen atom formed at the point of dissociation has a majority of the positive charge, we then assign the dynamics to the $O + N^+$ channel. The same approach can be applied to the $O^+ + N$ channel. Figure 4 shows probabilities of nondissociative and dissociative reactions on different dissociative charge states as a function of excitation laser pulse length. The laser field is aligned along the molecular axis with $E_{max} = 0.05$ au (~9×10^{13} W/cm^2), $\omega = 0.6$ au. Five different pulse lengths are investigated with respect to the laser control mechanism. With short laser pulses (<40 fs), nondissociative reactions account for >98% of the product. For dissociation reactions, the probabilities for $N^+ + O$ and $N + O^+$ channels are dependent on pulse length. As the pulse length increases, the probability of observing dissociative reactions of NO^+ also increases, from 0% with a 20 fs pulse to ~52% with a 100 fs pulse. The probability for forming the $O + N^+$ channel is approximately twice as likely as the $O^+ + N$ channel for dissociative reactions at all pulse

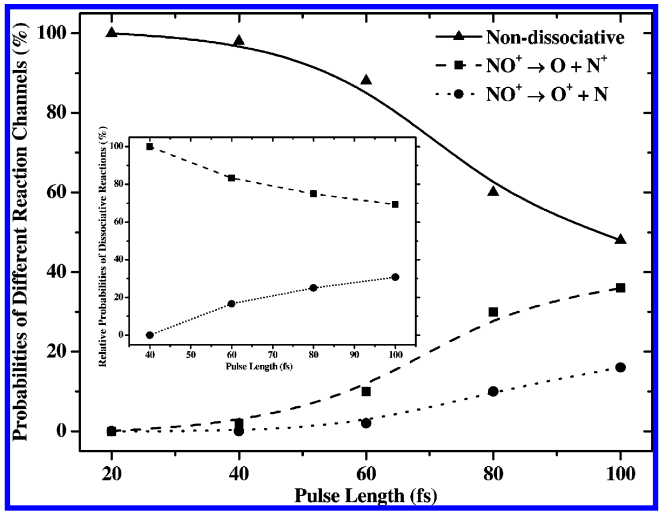

Figure 4. Probabilities of dissociative charge states of NO^+ as a function of applied pulse length. The field is applied along the molecular axis with $\omega = 0.60$ au, $E_{max} = 0.05$ ($\sim 9 \times 10^{13}$ W/cm^2). As the pulse length increases, the probability of dissociative reactions increases, while the relative probability of reactions that correspond to the $O^+ + N$ channel also increases.

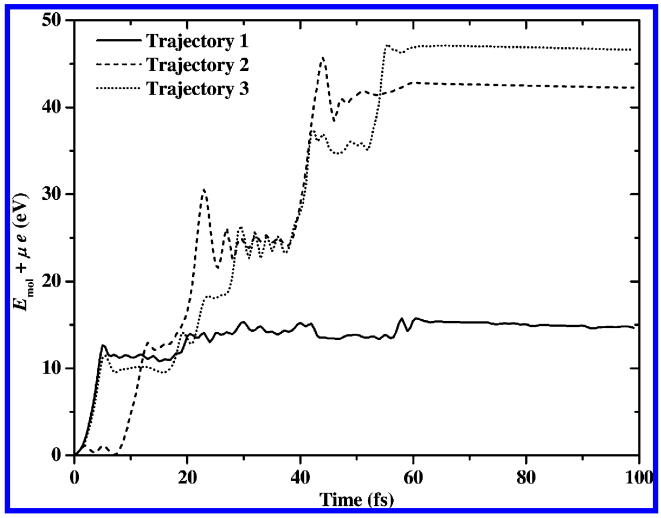

Figure 5. Total energy of the molecule (E_{mol}) plus the electric-dipole coupling ($\mu \cdot e$) as a function of reaction time for three select trajectories with a 60 fs laser pulse, $\omega = 0.60$ au, $E_{max} = 0.05$ ($\sim 9 \times 10^{13}$ W/cm^2).

durations. Although this observation presents an interesting target for the control of desired dissociation products with tailored pulse length, the mechanism of this effect remains to be clarified.

Figure 5 shows time-dependent total energies of the reaction system itself from three representative electron−molecule Ehrenfest dynamics simulations with a 60 fs pulse. The total energy, calculated using eq 10, includes "on-the-fly" molecular kinetic energy, the electronic energy using the instantaneous electron density, and the electron-field coupling within the dipole approximation. The large stepwise jumps in energy clearly indicate electronic excitations upon absorption of resonant photons. The vibrational time period of NO^+ is $\sim$14.3 fs, suggesting that the time-delay between excitations is modulated by molecular vibrations as the resonant excitation has to coincide with the time-dependent potential energy gap. If the initial vibrational condition does not give rise to resonant absorption, it will take some period of time before the molecule vibrates to a certain position

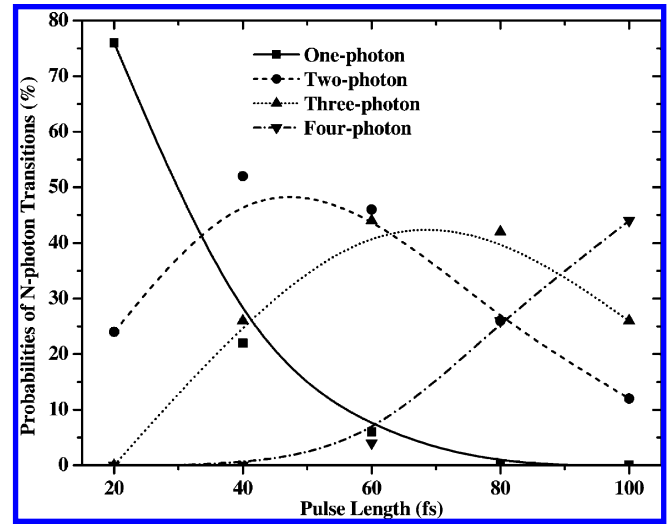

Figure 6. Probabilities of sequential multiple photon absorption processes as a function of laser pulse length.

that can lead to resonant absorption. The smaller amplitude oscillations during the time evolution are important characteristics of adiabatic electron dynamics on a given *dressed* potential surface. These oscillations are faster than the fundamental molecular vibration, but slower than the external driving field. Simple Rabi oscillation model can be used to understand this phenomenon. From linear response TDDFT calculations, the transition dipole moment for excitation from the ground state to the doorway excited state is 0.61 au. With laser field parameters used in this work, the fundamental Rabi frequency is calculated to be 0.05 au (2.9 fs in time period). This frequency agrees with those smaller oscillations in Figure 5. As the dynamics moves away from the resonant region after a large stepwise jump, the Rabi oscillation amplitude slightly decreases as expected.

By identifying the number of jumps in the energy time-evolution during the simulation, multiple photoabsorption processes can be analyzed. As a result, the observed excitations can be thought of as sequential multiple single-photon processes as plotted in Figure 6. Within a 20 fs pulse, the molecule can only undergo $\sim$1.4 vibrational cycles ($\nu = 2328.3$ cm^{-1}), therefore the resonant one and two single-photon processes dominate. However, as indicated in Figure 2b, the Stark-shifted or strong-field dressed lower lying PESs are mostly attractive potentials. Our simulations also suggest that the probability of observing dissociation with a 20 fs pulse is rather small for the NO^+ molecule. As the laser pulse length increases, the molecule is able to undergo more vibrational cycles and undergo multiple resonant excitations. There thus exists an optimal pulse length associated with the maximum probability of a certain multiple single-photon process. For example, the probability of absorption of two photons is highest with a 40 fs pulse, whereas the three photon process dominates with a 60−80 fs pulse. This relationship between multiple single-photon processes and laser pulse length can be used to explain the observed laser control pattern in Figure 4. As indicated from the molecular orbital (MO) density of states (DOS) plot in Figure 7, most lower-lying (from −15 to $\sim$0 eV) empty MOs show more positive charge built-up on N than on O, indicating a higher probability to access the $N^+ + O$ channel for lower energy excited states. On the other hand, there are a significant number of MOs that correspond to the $N + O^+$ dissociation channel among higher energy (>0 eV) empty MOs. As the

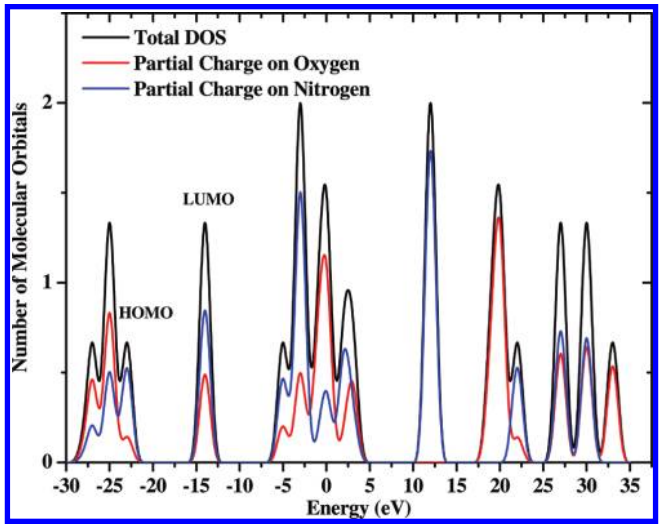

Figure 7. Density of state plot of molecular orbitals of the ground state NO^+. Partial charges on N and O are plotted as colored lines. In the lower energy regime (−15 to 0 eV), most MOs are related to the $N^+ + O$ channel, whereas higher energy (>0 eV) MOs see higher probability to access the $N + O^+$ dissociation channel.

pulse length increases, probabilities of multiple single-photon processes increase and the probability of accessing higher energy PESs also increases. As a result, the likelihood of the dissociative products coming from the $N + O^+$ channel increases with longer pulse lengths. This analysis provides an important control mechanism for the fundamental photoabsorption processes with a controlled laser pulse length.

Because the method used in this work is constrained within a single Slater determinant, proper symmetry-adapted singlet excited states cannot be obtained during the dynamics. Excitations observed in this work correspond to simultaneous spin-up and spin-down two-electron transitions.[36] As a result, the multiple single-photon processes as discussed above apply simultaneously to both spin-up and spin-down electrons and are below the double ionization potential. With the external field used in this paper, the Keldysh parameter[37] is calculated to be ∼27, suggesting possible multiphoton ionization. However, even with the 100 fs pulse, we did observe energies that were close to or above the double ionization potential of NO^+. This work introduces a mechanism of using laser pulse length to control photoabsorption probabilities. Although the intensity of the field is important for simultaneous multiphoton absorption processes, theoretical observations herein show that sequential single-photon processes can be controlled with tailored pulse length.

V. Conclusion

In this paper, we present first principles studies of laser-controlled dissociative charge states of NO^+ using TDDFT Ehrenfest dynamics with an electric field pulse within the dipole approximation. Intense electric fields with five different pulse lengths were compared, combined with PES and DOS analysis, to understand the effect of pulse length on the control mechanism. With a shorter pulse length field, the probability of absorption of one or two photons is highest, and the dominant dissociative charge state corresponds to the $N^+ + O$ reaction channel. As the pulse length increases, probabilities of multiple single-photon processes increase and the likelihood of the dissociative products coming from the $N + O^+$ channel also increases. This work introduces a concept of using laser pulse length to control the sequential multiple single-photon process. By showing the correlation between the laser pulse length and the probability of sequential multiple single-photon processes, this important concept provides initial groundwork for future optimizations of laser control mechanisms.

Acknowledgment. This work is supported by the National Science Foundation (CHE-CAREER-0844999, PHY-CDI-0835546), and the University of Washington Student Technology Fund.

References and Notes

(1) Rice, S.; Zhao, M. *Optical Control of Molecular Dynamics*; Wiley Interscience: 2000.
(2) Shapiro, M.; Brumer, P. W. *Principles of the Quantum Control of Molecular Processes*; Wiley Interscience: 2003.
(3) Chelkowski, S.; Bandrauk, A. D. *J. Chem. Phys.* **1993**, *99*, 4279.
(4) Talebpour, A.; Bandrauk, A. D.; Vijayalakshmi, K.; Chin, S. L. *J. Phys. B, At. Mol. Opt.* **2000**, *33*, 4615.
(5) Padgett, M.; Allen, L. *Physics World* **1997**, *10*, 35.
(6) Levis, R. J.; Menkir, G. M.; Rabitz, H. *Science* **2001**, *292*, 709.
(7) Bardeen, C. J.; Yakovlev, V. V.; Wilson, K. R.; Carpenter, S. D.; Weber, P. M.; Warren, W. S. *Chem. Phys. Lett.* **1997**, *280*, 151.
(8) Kleiman, V. D.; Arrivo, S. M.; Melinger, J. S.; Heilweil, E. *J. Chem. Phys.* **1998**, *233*, 207.
(9) Pastirk, I.; Brown, E. J.; Zhang, Q. G.; Dantus, M. *J. Chem. Phys.* **1998**, *108*, 4375.
(10) Yakovlev, V. V.; Bardeen, C. J.; Che, J. W.; Cao, J. S.; Wilson, K. R. *J. Chem. Phys.* **1998**, *108*, 2309.
(11) Legare, F.; Chelkowski, S.; Bandrauk, A. D. *Chem. Phys. Lett.* **2000**, *329*, 469.
(12) Elliott, D. J.; Townsend, P. D. *Philos. Mag.* **1971**, *23*, 261.
(13) Hattori, K.; Okano, A.; Nakai, Y.; Itoh, N. *Phys. Rev. B* **1992**, *45*, 8424.
(14) Nakai, Y.; Hattori, K.; Okano, A.; Taguchi, T.; Kanasaki, J.; Itoh, N. *Surf. Sci.* **1993**, *283*, 169.
(15) Kanasaki, J.; Ishida, T.; Ishikawa, K.; Tanimura, K. *Phys. Rev. Lett.* **1998**, *80*, 4080.
(16) Hess, W. P.; Joly, A. G.; Beck, K. M.; Henyk, M.; Sushko, P. V.; Trevisanutto, P. E.; Shluger, A. L. *J. Phys. Chem. B* **2005**, *109*, 19563.
(17) Dantus, M. *Annu. Rev. Phys. Chem.* **2001**, *52*, 639.
(18) Gauduel, Y. *Actual. Chim.* **2001**, 3.
(19) Li, X.; Tully, J. C.; Schlegel, H. B.; Frisch, M. J. *J. Chem. Phys.* **2005**, *123*, 084106.
(20) Isborn, C. M.; Li, X.; Tully, J. C. *J. Chem. Phys.* **2007**, *126*, 134307.
(21) Smith, S. M.; Romanov, D. A.; Li, X. S.; Sonk, J. A.; Schlegel, H. B.; Levis, R. J. *J. Phys. Chem. A* **2010**, *114*, 2576.
(22) Moss, C. L.; Isborn, C. M.; Li, X. *Phys. Rev. Lett.* **2009**, *80*, 024503.
(23) Isborn, C. M.; Li, X. *J. Chem. Theory. Comput.* **2009**, *5*, 2415.
(24) Liang, W. K.; Isborn, C. M.; Li, X. S. *J. Phys. Chem. A* **2009**, *113*, 3463.
(25) Erman, P.; Karawajczyk, A.; Rachlewkaline, E.; Stromholm, C. *J. Chem. Phys.* **1995**, *102*, 3064.
(26) Le Padellec, A.; Djuric, N.; Al-Khalili, A.; Danared, H.; Derkatch, A. M.; Neau, A.; Popovic, D. B.; Rosen, S.; Semaniak, J.; Thomas, R.; af Ugglas, M.; Zong, W.; Larsson, M. *Phys. Rev. A* **2001**, *6401*.
(27) Settersten, T. B.; Patterson, B. D.; Gray, J. A. J. Chem. Phys. 2006, *124*,
(28) Polak, R.; Fiser, J. F. *Chem. Phys.* **2004**, *303*, 73.
(29) Zhong, Z. P.; Zhang, W. H.; Li, J. M. *J. Chem. Phys.* **2000**, *113*, 136.
(30) Hikosaka, Y.; Aoto, T.; Ito, K.; Terasaka, Y.; Hirayama, R.; Miyoshi, E. *J. Chem. Phys.* **2008**, *128*.
(31) Li, X.; Smith, S. M.; Markevitch, A. N.; Romanov, D. A.; Levis, R. J.; Schlegel, H. B. *Phys. Chem. Chem. Phys.* **2005**, *7*, 233.
(32) Frisch, M. J.; Trucks, G. W.; Schlegel, H. B.; Scuseria, G. E.; Robb, M. A.; Cheeseman, J. R.; Scalmani, G.; Barone, V.; Mennucci, B.; Petersson, G. A.; Nakatsuji, H.; Caricato, M.; Li, X. H.; Hratchian, P.; Izmaylov, A. F.; Bloino, J.; Zheng, G.; Sonnenberg, J. L.; Hada, M.; Ehara, M.; Toyota, K.; Fukuda, R.; Hasegawa, J.; Ishida, M.; Nakajima, T.; Honda, Y.; Kitao, O.; Nakai, H.; Vreven, T.; Montgomery, J. A. J.; Peralta, J. E.; Ogliaro, F.; Bearpark, M.; Heyd, J. J.; Brothers, E.; Kudin, K. N.; Staroverov, V. N.; Kobayashi, R.; Normand, J.; Raghavachari, K.; Rendell, A.; Burant, J. C.; Iyengar, S. S.; Tomasi, J.; Cossi, M.; Rega, N.; Millam, J. M.; Klene, M.; Knox, J. E.; Cross, J. B.; Bakken, V.; Adamo, C.; Jaramillo, J.; Gomperts, R.; Stratmann, R. E.; Yazyev, O.; Austin, A. J.; Cammi, R.; Pomelli, C.; Ochterski, J. W.; Martin, R. L.; Morokuma, K.; Zakrzewski, V. G.; Voth, G. A.; Salvador, P.; Dannenberg, J. J.; Dapprich, S.; Parandekar, P. V.; Mayhall, N. J.; Daniels, A. D.; Farkas, O.; Foresman, J. B.; Ortiz, J. V.;

Cioslowski, J.; Fox, D. J. *Gaussian Development Version, Revision G.01*; Gaussian, Inc.: Wallingford CT, 2009.

(33) Casida, M. E. Time-Dependent Density Functional Response Theory of Moleuclar Systems: Theory, Computational Methods, and Functionals. In *Recent Developments and Applications of Modern Density Functional Theory, Theoretical and Computational Chemistry*; Seminario, J. M., Ed.; Elsevier: Amsterdam, 1996; Vol. 4, pp 391.

(34) Stratmann, R. E.; Scuseria, G. E.; Frisch, M. J. *J. Chem. Phys.* **1998**, *109*, 8218.

(35) Hase, W. L. Classical Trajectory Simulations: Initial Conditions. In *Encyclopedia of Computational Chemistry*; Schleyer, P. v. R., Allinger, N. L., Clark, T., Gasteiger, J., Kollman, P. A., Scheafer III, H. F., Schreiner, P. R., Eds.; Wiley: New York, 1998.

(36) Isborn, C. M.; Li, X. S. *J. Chem. Phys.* **2008**, *129*, 204107.

(37) Keldysh, L. V. *Sov. Phys. JETP* **1965**, *20*, 1307.

JP102013B